Drag Reduction on car side mirrors with the implementation of camera modules

Fourth Year Engineering Thesis
Dr. Jeffrey Yokota

Ryerson University
Department of Aerospace Engineering
10 April 2020

Mahmud Hasan
500 710 148

Acknowledgements

I would like to express my special thanks to my advisor Dr Jefferey Yokota, for the guidance he has provided in the conduction of this project. I am eternally grateful for this opportunity to have learned such skills which I wish to further develop in the near future.

I would also like to thank the Ryerson University for having provided the facilities for the conduction of the Computational Modelling, and the support of my fellow classmates for their continued support and cooperation in the conduction of the many overnight simulations.

Abstract

The greatest obstacle in the acceleration of a car through air is aerodynamic drag. With this increased drag is the expenditure of fuel. About 50-60% of a vehicles' total fuel energy is lost to overcome adverse aerodynamic forces. However, with the increase of fuel prices, many solutions have surfaced. One of these solutions are the implementation of camera modules to replace bulky traditional side mirrors. For this report, a thorough analysis was conducted into the aerodynamic benefits of these newly proposed camera modules in comparison to the conventional solid state mirrors. Specifically, one conventional side mirror along with two newly proposed camera module's were studied in this thesis report.

For this analysis, the overall drag of each module was found using CFD simulation under turbulent conditions at 60 km/h using the Realized K-ϵ method. The drag and C_d values found for the conventional side mirror were 3.985 N and 0.38 respectively. The values found for the two camera modules, Models B and C, were 0.526 N and 0.857 N. Their C_d values were found to be 0.312 and 0.365. This shows a potential of the drag reduction of the side mirror by almost 87% if the switch was made to the newer technology. This value also agreed with the prediction by Honda on their technology which has stated a possible drag reduction for this part by up to 90%.

However, when observing the bigger picture, it became evident that although this drag reduction is significant for locally, it simply is not enough to make a big impact on the drag reduction of the entire vehicle. With a maximum decrease in the total vehicle drag found to to be only 4%, the reduction in the fuel consumption of the vehicle would only decrease by 0.2 gallons per mile. On the other hand, improvements in parts such as the car rims or the underbelly of the car can result in fuel improvements of upwards of 12%-25%. For this reason, it can be concluded that automobile manufacturers research other possible solutions to reduce the vehicle drag such as with the redesign of the underbelly of the car or wheel arches and rims.

Contents

List of Figures

List of Tables

Chapter 1

Introduction

1.1 Purpose

Aerodynamic drag of cars has probably received highest attention over last five decades in experimental and practical fields of fluid dynamics [3]. With this, researchers have looked into the reduction of different forms of drag as well as the reasons behind them. This led to the redesign of car parts such as the cars rear wings, diffuser, underbelly, side body and most recently, the car side mirror.

With this, the design for camera modules to replace side mirrors was concocted and is currently on the market in Europe and Asia through automobile manufacturers ranging from Audi to Lexus. According to claims by Honda, the implementation of their rendition of the car side mirror reduces side mirror drag by 90% while decreasing the overall car‘s drag by 3.8% [4]. Not only is there aerodynamic improvements, but the implementation of this new design also increases the field of vision of the side mirror by 50% and effectively removes the vehicles blind spot for increased safety in operation.

Regardless of benefits, the National Highway Traffic Safety Administration has disallowed for the implementation of this camera module in any vehicle in North America as a potential replacement to the existing solid state mirrors [5].

This report will serve as a study into possible design iterations which can be had into current side mirror designs to see if there is any possibility for the solid state side mirror to reach the same level of drag reduction as can be achieved by the camera module. If not, arbitrary designs will be created to see the best possible improvements which can be made to the overall car's aerodynamic performance.

For this, the current markets' side mirrors will first be analysed alongside futuristic mirror-free side modules. Following, a redesign will be attempted to see if there are any improved drag benefits from changing the geometry of any of the tested side mirror models. From these local calculations, a transfer needs to be made relating the aerodynamic improvements on the side mirror to improvements on the car as a whole. With this, a decision can be made on if research into this sub sector of automobile design should be further investigated or if aerodynamic efficiencies from other components of the car are more beneficial.

1.2 Analysis Method

For the design problem at hand, there are several ways which the problem can be tackled. As a summary, this report will look to analyse aerodynamic properties associated with several designs. Listed are several ways that this can be done.

- Hand Calculations/MATLAB Computation
- 3D Printing + Wind Tunnel
- Computational Modelling

Firstly, using hand calculations for this design process, although may be possible for estimation purposes, will prove to have too many flaws as well as be beyond the scope of what can be learned in the course of the year. If hand calculations were to be done, a drag coefficient for each of the side mirror models would first need to be found then using the drag equation, the total drag can be found. However, trying to find pressure drag and skin friction drag separately would prove to be a challenge. These specifics will be further discussed throughout this report. A report written on finding the drag coefficients of arbitrary shapes illustrated the complexity of this procedure and therefore proved to be enough of a reason for this method to be avoided [6]. In general, this is a bad idea.

3D printing each side mirror module and putting the models in a wind tunnel is a very efficient way of computing the drags of each part. For the drag computation, pitot tubes can be put in the flow stream aft of the part and pressure distribution can be viewed find the drag on the system. Like the previous method, this will also require a lot of tedious calculations when dealing with the pressure distribution. This method will also require for the printing of parts which will not be effective depending on how many models will be made. If there are only four or five models being made then printing is cost effective, however, if there is a need for 10+ models to be made and analysed, then printing can become expensive. In addition, to run each test would require for lab technician supervision and if there needs to be 2 tests run for each model, then a total of 20 tests would be required. This is not an effective use of the time of the technician.

The last method which was considered is using computational modelling for this design problem. This is the method which was selected due to the and independence that's associated with the use of such software. There is no real limit to the number of models which can be analysed using this method, nor is there a need for a professional to serve as a guide along the way. This method also allows for a lot of versatility in the computation. For example, a case set up for one velocity can be easily changed to a different velocity in a matter of seconds (not taking into consideration run time). This may not be the case with using a wind tunnel where there may be a limit to how many times a week the university's facilities can be used and when the lab technician is available. For this method, the softwares which will be used are CATIA for the 3D modelling and ANSYS Fluent for the Computational Fluid Dynamics modelling.

1.3 Report Breakdown

This report will explore the differences between the current design of the side mirror on passenger vehicles and compare them to the new camera modules used as a replacement for side mirrors. The initial steps for this project will therefore be to design or acquire appropriate 3D models to be tested.

Tests for these side mirrors then need to be done to find appropriate drag values. These drag values can then be compared. To see if the numbers are correct, comparison need to be made to engineering literature found online outlining appropriate drag values and drag coefficients of the models to be used.

If the models are correct, changes shall be made to the current camera-less side mirror to increase its aerodynamic properties via a reduction in drag. This can be done by reducing pressure drag or reducing skin friction drag.

Finally, a relationship between the vehicle being studied and its drag value needs to be made to the fuel consumption of the vehicle. Therefore, if an X percentage of drag is reduced, it would be useful to have a mile per gallon that can be saved. This can be seen below in Figure 1.3.1 outlining the general outline of the project at hand.

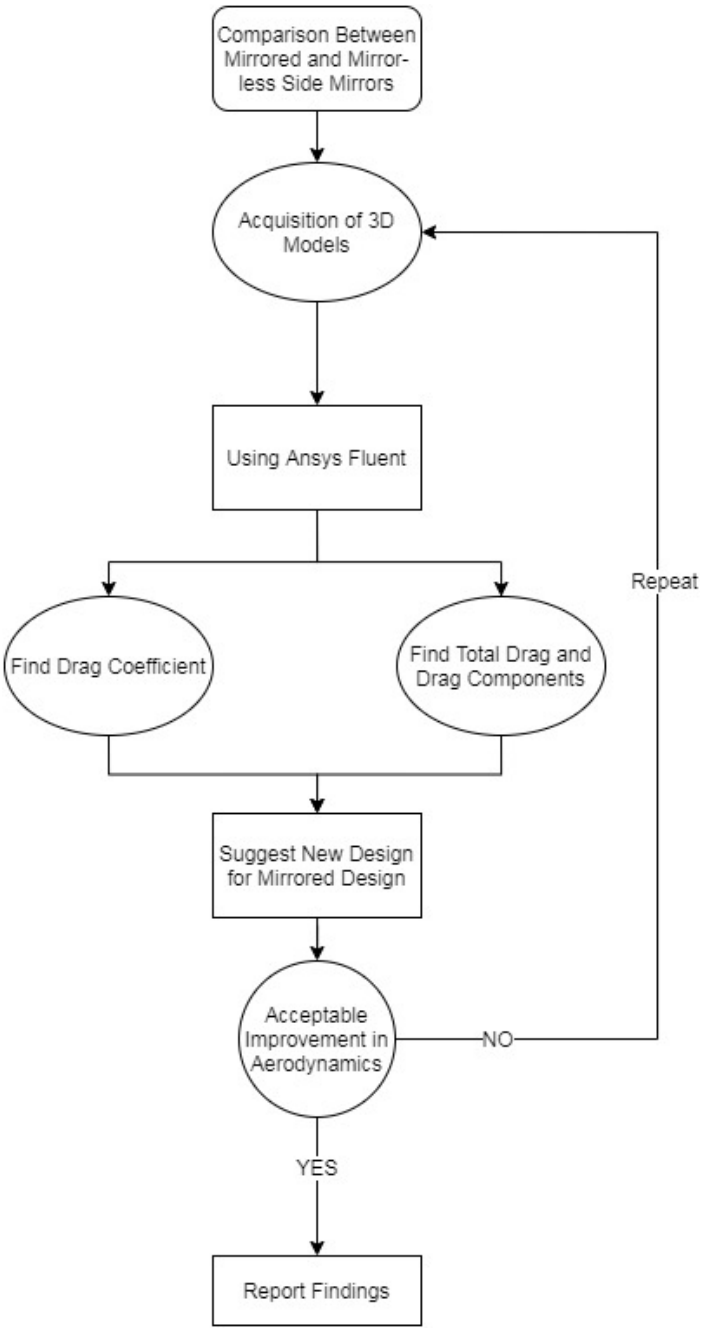

Figure 1.3.1: Thesis Workflow

Chapter 2

CATIA Modelling

2.1 Car Selection

Models of existing side mirror designs will be sought for as the purpose of this thesis is not to design modules from scratch. For simplicity, the cars which will be chosen for the analysis is the Lexus ES and the Honda E. Both these cars have the design parameters of their mirrors readily available online. These two manufacturers have both the mirror-less and mirrored variants of their side mirrors available online making the design process more accurate compared to having to design a part by eye.

Along with the camera modules for these cars, the side mirror module with the physical mirror is also needed. The tests will need to be run on this as the baseline. Unlike the side camera modules, the mirrored side mirror module for these two cars are almost identical and therefore a general 3D for the Honda will be used. Aerodynamic improvements to be compared are those relating to this base side mirror.

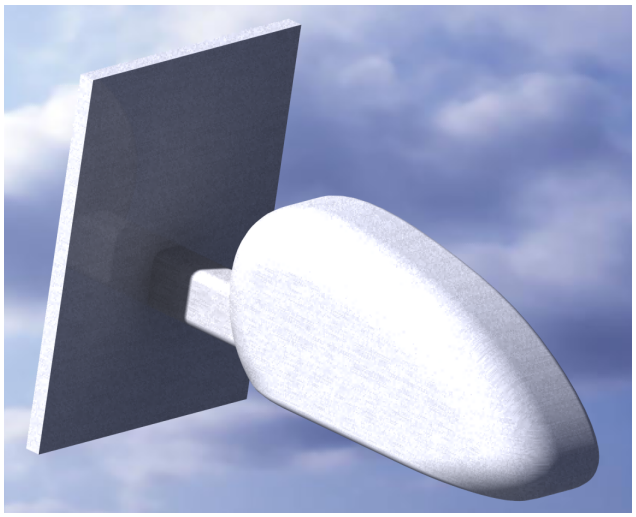

Figure 2.1.1: CAD Model of Side Mirror

The different side mirror modules which will be used through this report are the following. They can also be found in the Appendix.

- Generic Original Car Side Mirror **[MODEL A]**
- Honda E Side Mirror Camera Module **[MODEL B]**
- Lexus ES Side Mirror Camera Module **[MODEL C]**

For the modelling, a flat plate was added to each of these designs to replicate some sort of boundary layer interaction between the mirror and the 'car'. Although this isn't perfect, this will suffice for the time being. An investigation into changing the flat plate to one which better represented the whole vehicle was had but there seems to be no reason that the flat plate should not provide for accurate enough results for the analysis at hand. This is because this paper looks into the comparison between side mirrors amongst themselves and therefore given the same "door" to be mounted to, the results will be independent to the geometry of the plate. Therefore, rather than complicating the geometry of parts peripheral to the side mirror, the flow will just need to be adjusted to represent the turbulent behaviour caused by peripheral car parts in the vicinity of the car side mirror.

This report will also look to redesign the car side mirror by changing parameters associated with its geometry. To do this, a car side mirror will be chosen and its length (dimension parallel to the flow), and its cross sectional area (area perpendicular to the flow) will be changed. With these changes made, the effect on the side mirror's drag will be analysed. For this, the model in figure 2.1.1 will be used as a baseline to see the aerodynamic benefits that can be had by the implementation.

Chapter 3

Drag Calculation Procedure

For the comparison between different mirror designs based on aerodynamics, the drag will be compared. For this, the easiest parameter which can be studied is the drag coefficient of the design. As an example, a increase in the drag coefficient of a full-sized car of 0.01 can reduce the cars fuel economy by 0.2 mpg. The equation for drag can be seen below [7] in equation 3.1.

$$F_d = \frac{1}{2}\rho u^2 C_d A \tag{3.1}$$

where:

F_d = is the drag force, which is by definition the force component in the direction of the flow velocity,

ρ = is the mass density of the fluid,

u = is the flow velocity relative to the object,

A = is the reference area, and

C_d = is the drag coefficient – a dimensionless coefficient related to the object's geometry and taking into account both skin friction and form drag/pressure drag

The drag being computed is not a major concern when looking at low velocities but as can be seen by the drag equation in (3.1), the relationship between the velocity and the force of drag indicates that a vehicle travelling at 60 km/h will have four times the force working against its motion as opposed to a vehicle travelling at 30 km/h.

$$F_f = \int \frac{1}{2} C_f \rho u^2 dA \tag{3.2}$$

The above equation is related to the calculation of the skin friction over the surface of the vehicle. This is the viscous interaction between the solid and the fluid.
The tests which will be run on the models will be done at various velocities. For starters, a velocity of 60 km/h was chosen. The incoming air velocity will then be tested at highway speeds (100 km/h) for the sake of comparison. It will be interesting to observe what happens to the components of drag with these changing velocities. One thing to specifically look out for is around what velocity the flow starts to noticeably separate off the camera module being tested. This will give an indication of at which speed the drag will quickly increase. It can be assumed that the drag at the higher velocity will be much larger than that at the lower velocity simply off equation 3.1, but tests need to be done to find the relationship between the drag and velocity parameter. For the drag being observed, there can be a breakdown between the skin friction drag and the pressure drag

being observed by the body.

3.0.1 Skin Friction Drag

The skin friction drag coefficient is defined as follows:

$$C_{Df} = \frac{2D_f}{\rho V_\infty^2 S_{ref}} = C_f \left(\frac{S_{wet}}{S_{ref}} \right) \tag{3.3}$$

where:
D_f = Skin friction drag,
ρ = is the mass density of the fluid,
V_∞ = freestream airspeed,
S_{wet} = wetted area,
C_f = skin friction coefficient and,
C_{Df} = skin friction drag coefficient

Skin friction occurs when a fluid's viscosity flows over a surface. The magnitude of skin friction is dependent on the viscosity of the fluid and the wetted or total surface area in contact with the fluid. Another parameter is the roughness of the surface. Due to mixing in the flow as the flow transitions from laminar to turbulent, complications arise in the analysis procedure. This is called a mixed boundary layer. For the analysis at hand, the inlet will already provide for mixing in the flow and running turbulent models will also ensure that the flow is well mixed once it comes in contact with the side mirror by causing for separation in the flow [8]. The material to be used for the analysis of the side mirrors will be a hardened thermoset polymer. The same thermoset polymer will be used for all the side mirrors as the material selection is not of importance compared to the actual geometry of the side mirror. In addition, using the Reynold's number for the flow [found to be $2.28*10^{-5}$ in a following chapter], the estimated skin friction drag coefficient is depicted in equation 3.4 [8].

$$C_{Df} = 0.0743 Re_l^{-1/5} \tag{3.4}$$

Equation 3.4 is not the most accurate for the case being studied as it is for a turbulent flow over a smooth plate with a Reynold's number of $5*10^{-5}$, but for the case of the study, this is the closest representation. Fluent will however decide which equation is best to be used in every situation automatically depending on the corresponding Reynold's number and mixing in the flow [8]. This was one of the reasons that hand/MATLAB calculations would prove to be difficult for the analysis as equations and tabulated coefficients only correspond to known 2D and 3D geometries. The respective equation such as that in 3.4 for an arbitrary geometry such as that of a side mirror simply does not exist. Rather, simplifications or assumptions need to be made to get an approximate solution.

3.0.2 Pressure Drag

Pressure Drag is created by components of forces due to pressure acting normal to the surface of an object at all points.

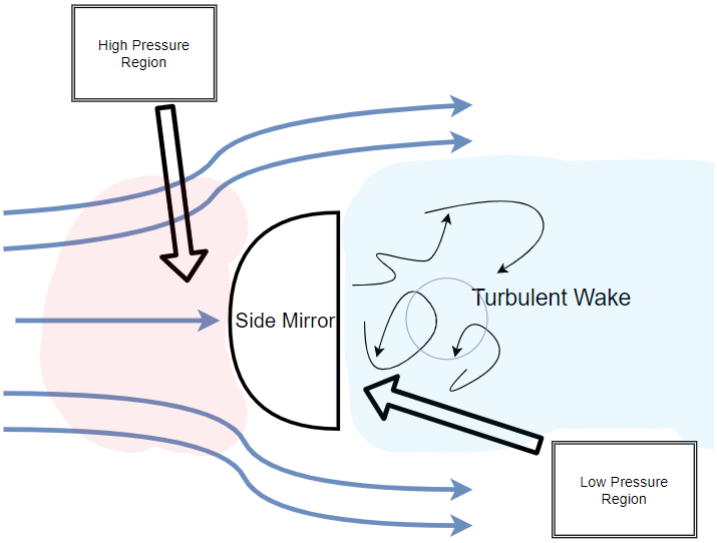

Figure 3.0.1: Pressure drag on a side mirror

For the calculation of pressure drag, the cross sectional area is used. Therefore, to reduce the pressure drag, efforts will be made to reduce this cross sectional area. Pressure drag is also of importance when observing a separated flow where the mixing caused by the turbulence creates large pressure differences before and aft of the object of analysis. Therefore, it can be expected that the side mirrors with a more aerodynamic profile correspond to those with lower pressure drags. Skin friction on the other hand is a function of the wetted area, rather than the cross sectional area. Therefore to reduce the skin friction drag, one can simply reduce the total surface area of the side mirror. Both of these techniques will be kept in consideration for the redesign process.

Chapter 4

ANSYS Set-up

4.1 Turbulence Models

The flow of the air as it goes past the side mirror can firstly be assumed to be turbulent. This is because the flow will have already travelled over the bonnet of the car, over the windshield and over the cars doors before reaching the side mirror. By this time, the air will have already mixed with itself to form a turbulent incoming airflow. This can be seen illustrated in Figure 4.1.1 which shows the change in the velocity of the incoming air as the streamlines become closer together. This change in the effective area will cause mixing in the flow.

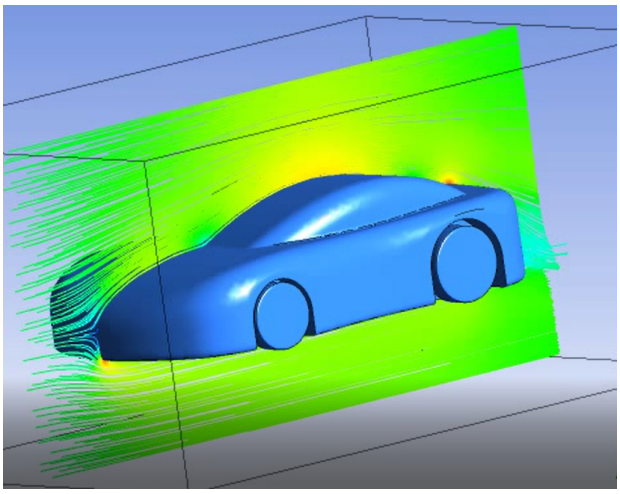

Figure 4.1.1: Sample Flow Modelled over a car body

Of the turbulent models, there are a few to choose from. Without delving too deep into the matter, engineering literature [9] was utilised to narrow down the range of solution methods to be used down to two. These two methods are the RANS K-ϵ Methods and the RANS Two Equation Standard K-omega method [10]. A quick discussion and comparison these two methods will be conducted.

4.1.1 RANS K-ϵ Method

Of the K-ϵ turbulence models, there are several which differ based on the equations used and the parameters used in them. Of this group, there are two K-ϵ models which will

be analysed; the standard and the realized. In the standard K-ϵ model, two variables are solved for, namely the k, the turbulent kinetic energy and the rate of dissipation of kinetic energy ϵ. [10] . This technique provides offers a good convergence and is typically used on external flows with complex geometries. In general, this is a good model for the case at hand.
The limitations imposed onto this model include [10]:

- No-slip walls
- Adverse Pressure Gradients
- Strong Curvatures
- Jet Flows

Although most of the items on this list will not drastically impact the mirror being modelled, there is a possibility that the limitation on modelling adverse pressure gradients will hamper the quality of the results when looking at the pressure drag caused by the designs.

This leads to the Realizable K-ϵ Method [11].The Realizable K-ϵ method is the default recommended model for mainstream external flow simulation [10]. This represents the most widely documented and well quantified model currently used in the industry. The Realizable method improves upon some of the faults of the Standard method with improved performance for planar surfaces, jets and streamline curvature [10]. This method also has improved performance when dealing with the boundary layer in cases of a strong adverse pressure gradient and separation. This is the k-ϵ method which will be used.

4.1.2 RANS K-ω Method

This is another popular two-equation model which pairs the rate of turbulent kinetic energy dissipation k, and specific rate of dissipation of kinetic energy ω.

In the industry, this model is popular model for use on turbo machinery simulations where vortexes form at wing tips of the rotating blades. The most significant advantage of this model is that it can be applied to get accurate readings through the boundary layer without complication or further modification [10]

Limitations of this method include:

- Difficulty in convergence when compared to the K-ϵ method
- sensitive to initial conditions

Doing further research on this, it is evident that this may not be the best method for the modelling external flow over the side mirror. Many of the use cases that exist in publications involve modelling internal flows as well as highly complex geometries, both of which are not the case for the side mirror modules.

For this reason, the K-ϵ Realized method will be used for the conduction of this thesis.

However, the k-omega method will be used to draw rough comparisons between the two methods in search of possible discrepancies in the modelling.
As a summary, the realizable K-ϵ method is used for most standard cases. However, when a accurate representation of the boundary layer is critical involving high turbulence and flow separation, the k-omega becomes preferential. The K-ϵ can only provide a crude estimate which is ample for problems where the solution is dependent on physical models more than the assumptions made with the turbulence model. As this is a design optimization, the K-ϵ would therefore be slightly preferential. However, for the sake of covering all bases, both the K-ϵ and k-omega models will be compared for a similar shape to gauge differences. This will be done in a following chapter.

4.2 Turbulent Boundary Layers

As mentioned in the previous section, the models used for this design problem are both turbulent flow models. Therefore, the most important parameter to consider is the way different models deal with the development of the boundary layer [1]. First an introduction and understanding on the definition of the boundary layer will be had.

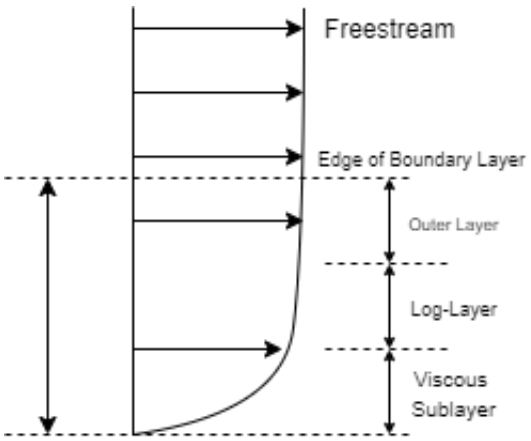

Figure 4.2.1: Turbulent Boundary sublayers [1]

According to the logarithmic law of the wall by Theodore von Karman, the average velocity of a turbulent flow is proportional to the logarithm of the distance from that point in the wall. Furthermore, the boundary layer is comprised of three different sub layers. Namely, the viscous sub layer, buffer layer, log-law inner layer and the outer layer. This can be seen displayed in Figure 4.2.1. This estimation can be extrapolated for being applicable for the entire flow, not just the portion of the flow close to the wall.
For CFD, the most important sub layer is the viscous sub layer directly adjacent to the wall and the subsequent log layer. The considerations made on sizing of the viscous sub layer will go on to directly impact the mesh sizing.
The boundary layer profile near the wall is such that the velocity changes logarithmically moving away from the wall. The dimensionless velocity follows the equation 4.1

$$\mu_\tau = \sqrt{\frac{\tau_{wall}}{\rho}} \tag{4.1}$$

Similarly, the wall distance is represented as follows in equation 4.1:

$$y^+ = \frac{y\mu_\tau}{\nu} \tag{4.2}$$

A further discussion on the significance of the y^+ value will be had shortly. By scaling the variables from the flow's interaction with the wall, the velocity profile data can be extrapolated, transitioning from linear in the viscous sub layer to a logarithmic behaviour in the log-layer [1].

4.3 Near Wall CFD Modelling Strategies

What was done in the original preliminary analysis of the side mirrors was a mesh was ensured to be fine for the purposes of encompassing the boundary layer without any further analysis to see whether the boundary layer was encompassed for the given turbulence model. This section will investigate this criterion through an investigation into wall functions used in ANSYS.

For the purpose of getting accurate results, the correct representation of the near-wall region is paramount. For this, ANSYS Fluent does the following for the use of wall functions and the resolution of the viscous sublayer. On the part of the user, the set guidelines need to be followed so as to abide by the grid sizing as outlined [1].

A) Using Wall Functions

- Wall functions use the dimensionless profile following equations 4.2 and 4.1 outlining the shear stress observed by the flow.
  - The first cell of the log layer falls within a y^+ value such $30<y^+<300$
  - For very high Re, the y^+ value usually can be higher whereas very low turbulent Re numbers, the log layer may not extend far away from the wall for the use of wall functions to still be accurate
- Wall functions should not be used if $y^+<30$

B) Resolving Viscous Sublayer

- The first cell should be at y^+ approximately 1 with a growth rate of approximately 1.2

Having done this, the mesh resolution near the wall will therefore need to be looked upon.

4.4 Near Wall Mesh Resolution

Of the two methods previously mentioned, methods A and B, the corresponding number of nodes near the wall differ. This can be seen illustrated below in figure 4.4.1.

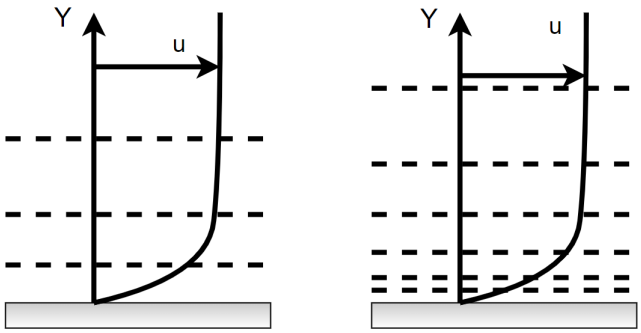

Figure 4.4.1: Near wall cell height of Log Based wall (Left) and viscous sub layers (Right) [1]

For both these cases, the first cell distance from the surface is determined by the computation of the y^+ value. This value needs to be inputted into ANSYS as it is a function of the model rather than of the flow. The computation for one of the side mirror models will now be demonstrated and its y^+ value found. With it, the approach that needs to be taken can be found. This early prediction can help to prevent any need for further remeshing of any of the models.

4.4.1 Computing Y^+ Value

For the side mirrors being analysed, the lengths are relatively the same with them varying from 10 cm to 20 cm in the direction of the flow. For that reason the Reynolds number should be very similar. The Reynolds number can be computed using equation 4.3.

$$Re_l = \frac{\rho V L}{\mu} \tag{4.3}$$

The values for the flow being analysed is a standard sea level densities, length of 20 cm and velocity of 16.66 m/s from the 60 km/h assumed speed of the car. It has to be noted that this equation assumes that the object in the flow is a flat plate. The resulting Reynold's number is approximately 2.28 * 10^5. If a different side mirror model were to be used, then the length (L) would change, however, the magnitude of the Reynold's number would remain the same. This also shows that the flow is clearly turbulent. For the remainder of the calculation, the required wall spacing will be computed for an aimed y^+ value of ≈ 50 [1].

To solve equation 4.2, the μ_τ needs to first be found. This velocity is defined by the following equation.

$$U_\tau = \sqrt{\frac{\tau_w}{\rho}}, \tau_w = \sqrt{\frac{1}{2} C_f \rho U^2} \tag{4.4}$$

The τ_w is the wall shear stress which is dependent on the skin friction of the surface. Using literature, this skin friction coefficient can be further simplified to be represented by equation [1] 4.5.

$$C_f = 0.058 Re_l^{-0.2} \tag{4.5}$$

The C_f value is found to be 0.00492, a τ value of 0.836 $kg/(ms^2)$ and a U_τ value of 0.83 m/s. Finally, the rearrange equation 4.2 gives the first cell height to be 0.88

mm.Therefore, the first cell height should be at least 1 mm. If a different y^+ value was aimed for, the first cell height would not be drastically different. For example, if a y^+ corresponding to a high Re number such as 200 was aimed for, then the required first cell height would be approximately 4 times larger than that found with the y^+ value of 50 used in this computation. Therefore, regardless of either case, a first cell size of 1 mm will suffice.

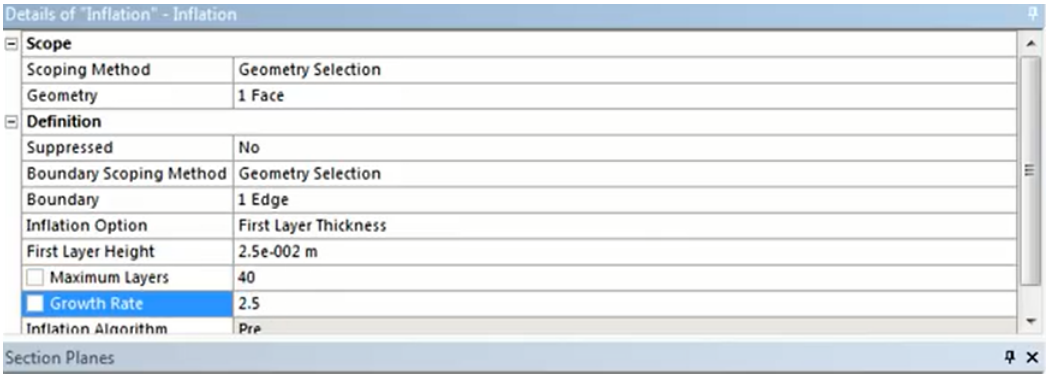

Figure 4.4.2: The first layer thickness in ANSYS

In ANSYS, the first layer thickness can then be set to a desired value with a growth rate set so that the other cells are not required to be as small as seen in figure 4.4.2. In addition, ANSYS also has setting where the max face size can be limited so the cell sizes do not become too large in the fluid domain .

4.5 Mesh Quality in Fluid Domain

The previous discussion looked upon how the mesh resolution is required to be near the walls. However, what about the mesh in all other parts of the flow? This section will look into how the mesh should be sized to efficiently get accurate results through experimentation and a trial and error method. The model which will be used for this is an earlier prototype for the side mirror used for Model A. As this part of the analysis looks at the set up relating to the mesh's, the exact geometry is not as important as these meshes should work for all of the side mirror modules independently of geometry.

The fineness of the mesh would help better encapsulate the interactions between the flow and the mirrors being analysed. In general, the finer the mesh, the more accurate the results will be (given all other components in analysis was done correctly). At the same time, the mesh shouldn't be overly complicated to the point where there is diminishing returns when comparing computing time and the accuracy of the results. For this reason, a simple test was devised to compare the drag values over the mirrored camera module.

Now with a turbulence model selected [K-ϵ realized], sample calculations can be run. Initial tests were run with a mesh that had a *Medium* Relevance Center and a Relevance of of -100. This results in a total node count of *11622* and *23248* elements.

Now, with a mesh with a *Fine* Relevance Center and a Relevance of *100*, the total node count of *379245* and *596832* elements.

The refinement from the coarse mesh to the fine mesh is to the order of approximately 33 times. In terms of processing time, the running of ten iterations with the coarse mesh took 4 seconds, compared to the running of ten iterations with the fine mesh taking slightly longer than 2 minutes.

The drag values which were found from the two runs for the model were found to be 2.2890 N for the coarse mesh and 2.9217 N for the fine mesh. This is a difference of almost 27%. This is much higher than what is acceptable if it is assumed that the finer mesh provides a "correct" answer while the coarse mesh provides an "incorrect" answer. The cause for this simply may be because part of the boundary layer being analysed is too small to be analysed by the elements in the coarse mesh. In other words, the distance between the nodes may be so large in comparison to the boundary layer thickness, that the skin friction drag at that instance is not computed. The finer mesh simply can pick up on more of these missed boundary layer interactions between the fluid and the surface of the mirror module, and therefore report back a higher drag value. This was one of the most important reasons that the y^+ value was computed earlier.

It can be noted that the improvements in the designs to be iterated will most likely be small, and therefore slight imperfections in the computation of the values can give incorrect end results.

It is with this, the decision was made for the comparisons between the models to use the finest mesh possible. Although further complications can be made into refining the mesh at certain areas of each design, by changing element sizing at edges and curves or by increasing the node count at points of interest, the mesh will be kept simple without these considerations made. This way, the same meshing initialization can be made on all models and result in similar node and element counts as long as the minimum of the first layer thickness is agreed upon by the required y^+ value.

Table 4.1: Coarse mesh vs. Fine Mesh in the computation of Overall Drag

Parameter	**Coarse Mesh**	**Fine Mesh**
Element Count	11 622	379 245
Node Count	23 248	596 832
Computation Time	4 seconds, ten iterations	124 seconds, ten iterations
Computed Drag (N)	2.289	2.921

A summary of the values found during these test runs can be seen above in Table 4.1. Although the run time for the finer mesh is one which is far longer than that of the coarse mesh, for the sake of accuracy in the results, time will have to be lesser of the concerns. This will be seen again when looking upon the number of iterations which should be run in section 4.8

4.6 Mesh Quality Parameters

The previous sections looked into the node count and the first cell sizes. Although these numbers are important, they do not say whether the mesh being constructed is "good" or "bad". A few of these metrics to gauge the mesh will be discussed in this chapter, namely the orthogonality, skewness and aspect-ratio.

4.6.1 Orthogonality

The orthogonality of the mesh looks into seeing how close adjacent angles are to the optimal angle. For example, if an angle between two intermediate faces is supposed to be 90, the orthogonality is a measure how close that angle is to the desired angle. The orthogonality scale measures a range from bad (0) to good (1) [12].

The orthogonality corresponds to the following equation relating the angle in degrees between the connection vector of the cell centers and the normal vector of the inner face, represented by C and f vectors in the equation.

$$min\left(\frac{A_i f_i}{\left|\vec{A_i}\right|\left|\vec{f_i}\right|}, \frac{A_i c_i}{\left|\vec{A_i}\right|\left|\vec{c_i}\right|}\right) \tag{4.6}$$

This can be seen further illustrated in figure 4.6.1. The orthogonality of the meshes used for this analysis ranged between 0.88-0.93, all within an acceptable range.

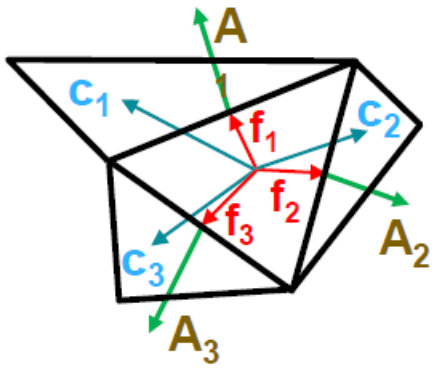

Figure 4.6.1: Cell center and normal vectors used for the computation of cell orthogonality

4.6.2 Skewness

Where orthogonality looked at the angles, skewness looks at the deviation of an element from an optimal equilateral volume. This is represented by equation 4.7.

$$Skewness = \frac{optimalcellsize - cellsize}{optimalcellsize} \tag{4.7}$$

For the cells being investigated, according to Normalized Angle Deviation Concept, finding the minimum angle between two lines joining opposite mid-sides of the element can

allow for the computation of the skewness as represented in equation 4.8. The skewness metric ranges from 0 (good) to 1 (bad).

$$Skewness = max\left[\frac{\theta_{max} - \theta_e}{180 - \theta_e}, \frac{\theta_e - \theta_{min}}{\theta_e}\right] \tag{4.8}$$

This is illustrated in the below figure. It will be attempted in this report to ensure that the skewness does not exceed 0.3-0.5 [9] [1]

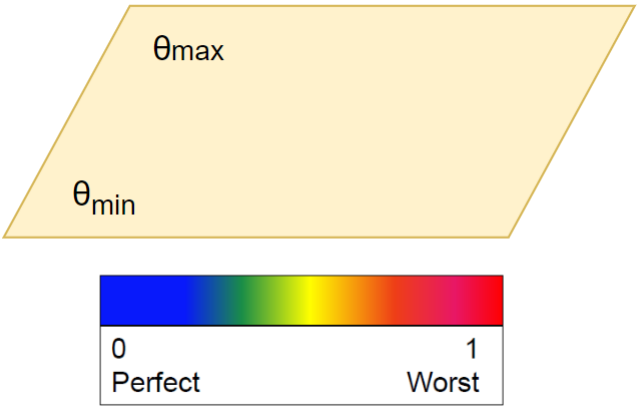

Figure 4.6.2: Normalized Angle Deviation Concept for the computation of the skewness

Like was found for the other parameters, the skewness of a sample mesh can be seen below in figure 4.6.3.

Quality	
Check Mesh Quality	Yes, Errors
Target Skewness	Default (0.900000)
Smoothing	Medium
Mesh Metric	Skewness
Min	1.0145e-003
Max	0.84183
Average	0.24232
Standard Deviation	0.11867

Figure 4.6.3: Skewness of a mesh around side mirror model A

4.6.3 Aspect Ratio

Lastly, the aspect ratio of the mesh is defined as the length to height ratio in 2D. In a 3D case, it is the radius ratio of a circumscribed to the inscribed circles. This is illustrated in figure 4.6.4. For accuracy, it is common for high aspect ratio cells for orthogonal layers near solid boundaries. Relaxation factors will need to be in place for the cells further from the boundary between the solid and the fluid. The aspect ratio of a triangle, tetrahedron, prism and hexa elements are all slightly different but for the purpose of this report, it will not be further elaborated as there is no exact metric for the measure of aspect ratio [12].

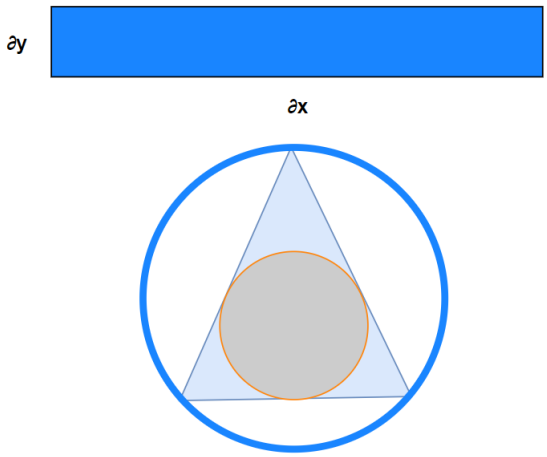

Figure 4.6.4: Aspect ratio

4.7 Inlet Boundary Conditions

The incoming flow onto the side mirrors will already be mixed and turbulent. This is a reasonable assumption as the flow will be travelling over the hood of the car, car's windshield and be interacting with the side door. For the CFD modelling, this incoming air must therefore have its inlet boundary conditions considered.
The following methods are used for the modelling of inlet turbulence conditions:

1. Turbulent Intensity and Viscosity Ratio (default)
    - The default values for the turbulent intensity and viscosity ratio are 5% and 10.
2. Turbulent Intensity and length scale
    - Length scale can be used when information on specific boundary layer heights are available. This scale depicts the size of the large eddies containing the most energy.
3. Turbulent Intensity and Hydraulic Diameter
    - This is for internal flows and will not be looked upon for this analysis

For this analysis, as there is not specifics on the flow being observed, the default turbulent intensity and viscosity ratios can be used. The normal turbulent intensities range from around 1% to 5%. The higher percentage correspondents to nominal turbulence through a circular inlet whereas for external flows, lower turbulent intensities can be used. For external flows, the turbulent viscosity ratio can be assumed to be between 1-10. For the conduction of this report, the values used for the turbulent intensity and viscosity ratios will be 1% and 5 respectively.

4.8 Number of Iterations

The parameters used for the drag computations can be found in table 4.2 as was discussed in section 4.5. Initially, the number of iterations which were run was 10 000. However, this was proving to be incredibly time consuming as a lot of the initial runs were simply done incorrectly and therefore days were wasted. For that reason, moving forward with many of the calculations, the number of iterations were cut from 10 000 down to 1000. This however is not a reasonable decision if this reduction in the number of iterations comes at the cost of accuracy of the results and that is what will now be innvestigated.

Table 4.2: Drag Computation Parameters

Parameter	**Value**
Mesh Quality	Fine
Turbulence Model	K-ϵ Realizable
Number of Iterations	10 000
Computation Time	$\sim$36 hours
Convergence Criteria	10^{-6}

In addition, the convergence criteria of 10^{-6} was originally used as it was suggested by engineering literature[13]. Attempts were made to increase the accuracy of the results by running the simulation over a weekend but even at around 20 000 iterations, the residuals remained around 10^{-7}. This can either be a result of one of two things:

- Error in the meshing
- Computer not powerful enough

The possibility that there is an error in the meshing suggests that it is possible that the mesh is not fine enough to lead to results in the residuals to the degree of precision sought after. This would mean that the mesh would need to be slightly changed for each of the side mirrors to warrant for a better encapsulation of each of the modules' exterior shape. This would lead to even longer computation times.

The second possibility is that the computer is not powerful enough to get results to the precision being asked for. To solve this, a more powerful computer can be requested from the school.

Regardless, for the project at hand, the residuals do not need to be accurate to the 10^{-8}th power. Therefore, running the computation overnight is really not required.

To illustrate, the same computation was run three times at a different number of iterations, and as can be seen in table 4.3, the number of iterations does not change the values of drastically, unlike the changing of the mesh quality. It can also be noted that where the drag values suddenly change between 100 iterations and 1000 iterations, the drag remains much more stagnant between 1000 and 10 000 iterations.

Table 4.3: Drag Computation Parameters

Parameters	**Values**		
Number of Iterations	100	1000	10,000
Drag Values (N)	2.2596	2.8587	2.9398

For that reason, the number of iterations which will be followed through for the testing of each module is 1000 as this is precise enough to get residuals down to at least the recommended residual as well as not take too long so as the computation reaches a point of diminishing returns.

Chapter 5

Results

5.1 Test Run on Cylinder

To ensure that all the parameters mentioned in the previous section related to the set up procedure to ANSYS is correct, a sample 3D cylinder will be placed in the identical flow as that of the side mirror. This will be done as values related to the drag coefficient and drag values in general can be easily found for a cylinder. Therefore, it can be easily gauged if there are any errors in the set up by looking at a percent difference between the drag values tabulated and that found using the software. For starters, a cylinder of equal proportions to the side mirrors in question will be used. For this, a cylinder of dimensions 10 cm in diameter and 20 cm in length was created. This cylinder was then simply placed in the turbulent 60 km/h flow. It should be noted, that this cylinder was not attached to a "car side door" as was the case with the mirrors observed simply because there are no tabulated values for such an orientation and therefore, it would prove difficult to prove if the set up was indeed correct.

This computation will be done using a turbulent flow as well as a laminar flow simply because laminar flows are more predictable and therefore the values found from the computation should be almost exactly as tabulated. A turbulent flow will also be modelled and related to tabulated values as well.

5.1.1 Laminar Flow over Cylinder

This model was created using a laminar flow under the same conditions as those which will be applied to the side mirror. The Cd value found for this can be seen plotted in figure 5.1.1. Below the figure is a table outlining the tabulated value as found in Hoerner's reference textbook for the given Reynold's number [2] and that found in the computation.

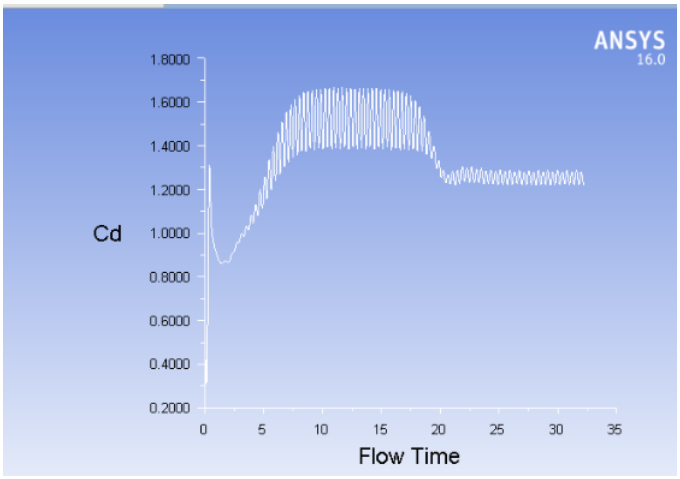

Figure 5.1.1: C_d of Cylinder in flow

Table 5.1: Computed Laminar C_d vs Reference Laminar C_d value [2]

	Computed Laminar C_d	**Hoerner's Reference Value**
C_d	≈ 1.27	≈ 1.2

The value found in the analysis provides a percent error of 5 as seen in table 5.1. This can be seen as acceptable for the conduction of this analysis. It can also be noted that these values are approximate as the conditions governing the analysis can change the drag coefficient slightly. For example, it is possible that with a higher number of iterations that the coefficient can fluctuate 0.02 as seen in the previous section pertaining to iteration count. The value tabulated in Hoerner's reference textbook also is presented with certain discrepancy as the value was read off a chart at a given Reynold's number.

Side Note: For further analysis, a transient model was also created to analyse the separation that is expected from the turbulent model. This can be seen in figure 5.1.2. Since the model used was transient, there appears to be von Karman vortices in the flow as can be seen in the figure to the right. This process of vortex shedding arises from unsteady separation of flow of a fluid around a blunt body. This phenomenon will most likely also present itself in the case of the side mirror [14].

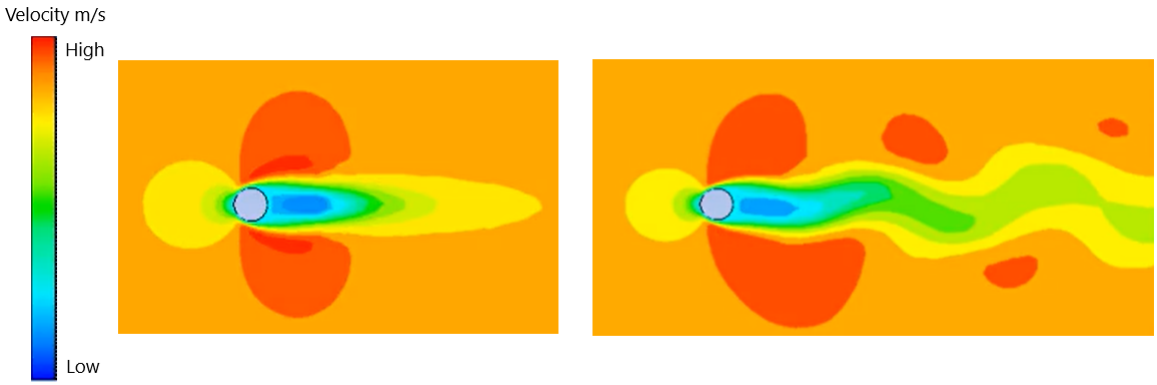

Figure 5.1.2: Velocity Contour with initial flow on the left and a flow at a later time step on the right

5.1.2 Turbulent Flow over Cylinder

Like was the case with the laminar flow, the turbulent flow will help verify if the preliminary steps taken to set up the ANSYS Fluent module was done correctly. This turbulent flow will closer represent what will be needed for the flow side mirrors' analysis. The found C_d value for this computation is that found below in table 5.2

Table 5.2: Computed Turbulent C_d vs Reference Turbulent C_d value [2]

	Computed Turbulent C_d	**Hoerner's Reference Value**
C_d	≈ 0.289	≈ 0.3

Like previously with the laminar flow case, the percent error is within acceptable margins (3.7%). With this confidence, the real models for the side mirrors can be used and their values found. The values for the side mirrors in terms of their drag coefficients should be very similar to the 0.289 found for the cylinder in the turbulent case. Also, another point to keep in mind is the turbulent coefficient of drag is dependent on the $\frac{L}{D}$ ratio where L represents the length of the cylinder and D represents the diameter of the cylinder [2]. As this ratio is increased, the drag coefficient and thus the overall drag reduces. However, there is a limit to which point the increase of this ratio benefits the drag reduction of the cylinder.

5.2 Drag Results

The testing included the analysis of the i) Generic Side Mirror ii) Honda E Side Mirror Camera Module and the iii) Lexus ES Side Mirror Camera Module.

These will be denoted as **Model A**, **Model B** and **Model C**. The models can be seen pictured in figure 5.2.1. These CAD models as mentioned previously are representations of real car side mirrors in market today. Further redesign of car side mirrors will be done in the following chapter Redesign.

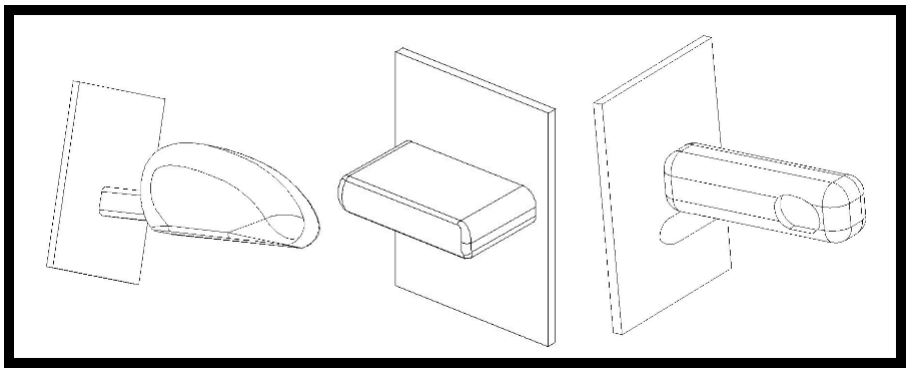

Figure 5.2.1: Isometric view of models A, B and C pictured left to right

The respective drag and drag coefficients for the Honda default side mirror [Model A] is tabulated online [4][15]. Therefore at least for Model A, the found drag values can be verified. As for the Honda E camera side module and the Lexus camera modules, Models B and C respectively, estimations need to be made with the information available online by the respective automobile manufacturers.

The drag of the entire shape was computed simply using the ANSYS software. This drag found combined the effects of both skin friction and pressure drag in each case and reported back a total drag value in Newton's. The software also computed a drag coefficient in each case. Listed below are all the findings in table 5.3.

Table 5.3: Drag Values Computed for the Different Models

	Model A	**Model B**	**Model C**
Drag (N)	3.985	0.5260	0.857
C_d	0.38	0.312	0.365

Are These Values Correct?

The legitimacy of each independent model should be validated to ensure that the numbers in table 5.3 are reputable. Therefore, where available, data found online by the manufacturer will try to be used to gauge if the accuracy of each of the calculations. It must be noted, due to the competitive nature of this industry, not all values and parameters are available online for all models.

Model A

Model A is simply the regular car side mirror. The information relating to this side mirror is readily available as the CATIA model for it was based of an existing vehicle (the Honda Fit). The hand calcualtion which can be done to verify the legitimacy of the numbers in Column 1 of table 5.3 are as follows.

Firstly, in the automotive industry, the complete vehicle drag is usually calculated based off the frontal area of the car [15]. This serves as a good reference area for the computations. To start off, the frontal reference area of the Honda Fit, off which Model A was based on, is 2.146 m^2. Along with this reference area, the C_d of the car can be found

online to be 0.35 [15]. With these values, an estimate for the cars drag can be found to be 127.689 N at standard sea level density and a velocity of 60 km/h using equation 3.1. Furthermore, the side mirror for the vehicle accounts for approximately 3% of the car's frontal area [16]. Therefore, it can be assumed that the drag from the side mirror accounts for approximately 3% of the entire vehicles drag, which would be 3.83 N. Although this methodology is very crude and doesn't consider the fact that the independent C_d's of different car parts vary, it can be seen that the 3.83 N estimated as the drag is very close to that found using the CFD model with a percent difference of 4%. Again, using 3.1, the C_d value can be verified in a similar manner.
This gives some additional confidence to the calculations.

Model B

Model B is slightly more challenging to calculate verify as there is no data online on the drag values on this component. However, according to Honda[4], this improved camera side module on the new Honda E claims to reduce the side mirror drag by 90%. This stated value can be used to give foundation to the calculated values in table 5.3.
Comparing the drag values between Model A and Model B, the drag for the second side mirror should therefore represent an improvement in the drag reduction by 90% [4]. This is very close as the overall drag value between the two models is reduced by 87%. It needs to be noted that Model A however is not exactly the side mirror which was used in the claim made by Honda but is similar enough to draw the comparison because the Honda E and the Honda Fit are vehicles of similar sizes and therefore have very similar, if not identical side mirrors.

Since the overall drag value seems to be accurate, the drag coefficient can also be assumed to be correct.

Model C

Lastly, the Lexus ES side mirror camera module is the only module for which no parameters exist online. Therefore, most of the verification that can be done for this last calculation are theoretical. However, given the accuracy of the previous two models, it is safe to assume that the values related to this model too, is correct. Observing the model for the Lexus side mirror visually, it can be assumed that the model be the most accurately simplified as a rectangular prism with rounded edges in the face of the flow. This simplification allows for the comparison between the drag coefficient found in the computation and those which are available in Hoerner's Reference Manual [2]. According to this reference, the C_d of such a shape in at the same Mach Number is ≈ 0.3. This is close to the value found. The computed drag coefficient however is larger in the case of Model C as along with a rectangular prism in the flow, there also exists a "side door" and a mount connecting the module to the car. These two extra objects in the flow would therefore increase the drag coefficient slightly from 0.3 as stated in the reference textbook [2].

The skin friction drag and the pressure drag were calculated separately for the calculation of the drag and the steps taken for each of these computations will be discussed in shortly in this section.

5.2.1 Skin Friction Drag

To find the skin friction of each module, the wall shear stress first needs to be found along the flow direction. Since drag is only in the direction opposite to flow, the shear stress on other walls of the modules can be ignored. The computation of this drag is formulated by Equation 3.2.

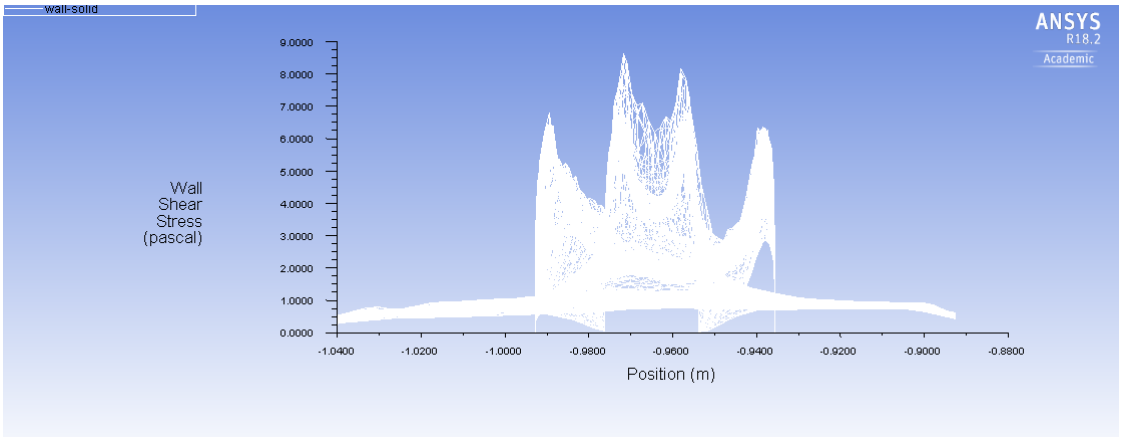

Figure 5.2.2: Model A wall shear stresses

The wall shear as can be seen in 5.2.2 and 5.2.3 for Model A and Model B.

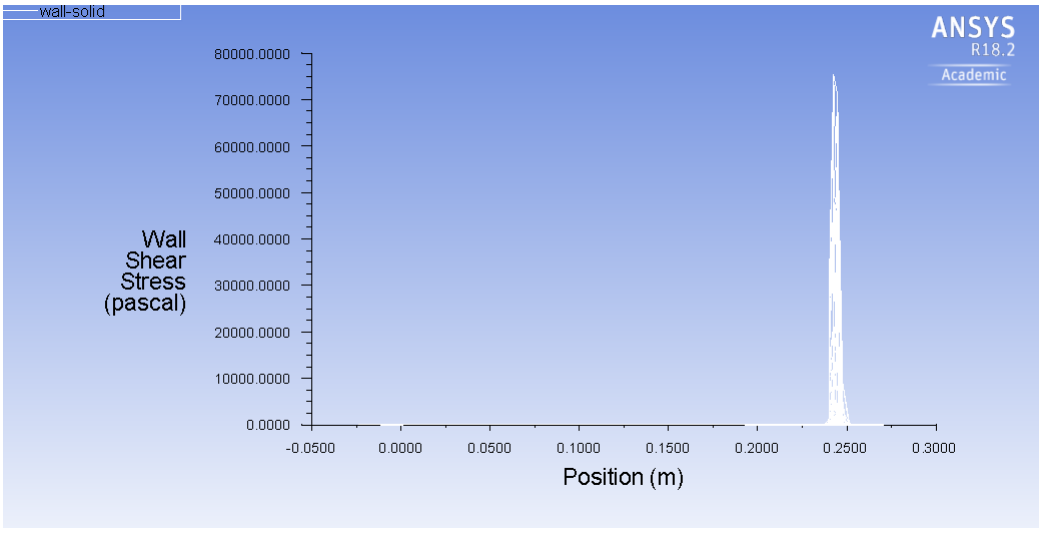

Figure 5.2.3: Model B side mirror module wall shear stresses

For a more visual illustration, contours can be used to illustrate the values relating to the wall shear stresses and pressure drag on the actual body of the side mirror. These are below in 5.2.4 and 5.2.5 for Model A and Model B respectively.

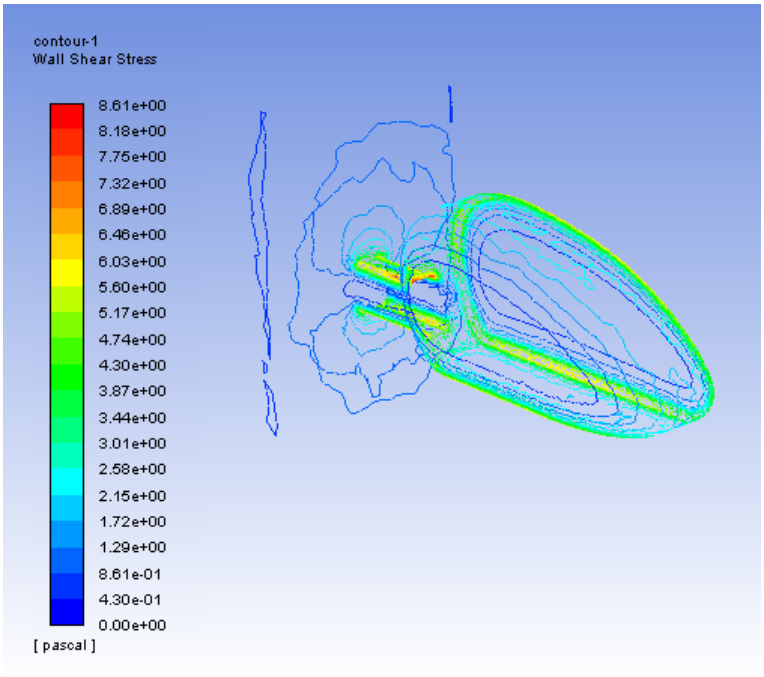

Figure 5.2.4: Contour illustrating the wall shear across surface of mirror, Model A

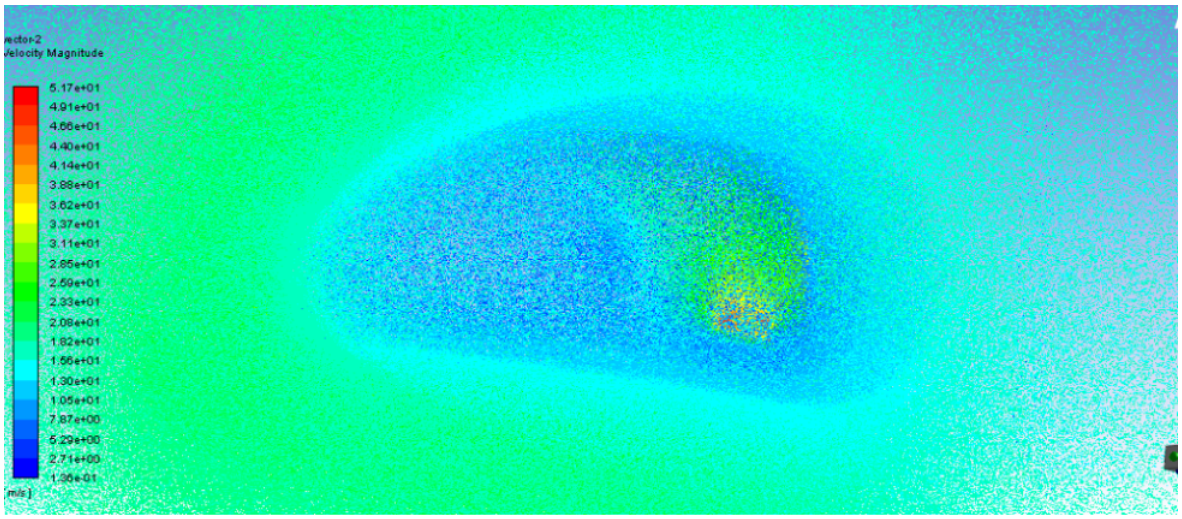

Figure 5.2.5: Velocity distribution across face of the side mirror, Model A

The velocity can be seen to be nearly zero at the surface while gradually growing larger to that of free stream away from the body. This is due to the face that the method used for this analysis uses a non-slip wall creating a boundary layer. It's due to the existence of this boundary layer that the skin friction values can be computed. This velocity distribution in this turbulent flow also causes for a variation in the pressure between the front and the back of the side mirror. This leads to pressure drag.

5.2.2 Pressure Drag

The pressure distribution across the surfaces of the modules can be observed and the differences in the values can be found to compute for the pressure drag component of

drag. The static pressure distribution along the flow direction can be seen below in figure 5.2.6. Like the skin friction drag, this has not yet been calculated correctly. For the computation of the pressure drag, the pressure differences across the frontal surface and the back of the mirror modules will need to be observed. It can however be seen in this graph that the pressure distribution in front and aft of the side mirror are almost symmetrical. This suggests that there is very little separation in the flow and due to this, the pressure drag will also be low. This can be seen in all the low drag coefficient values found for the three models analysed.

Below in figure 5.2.6 the pressure distribution can be seen for Model B.

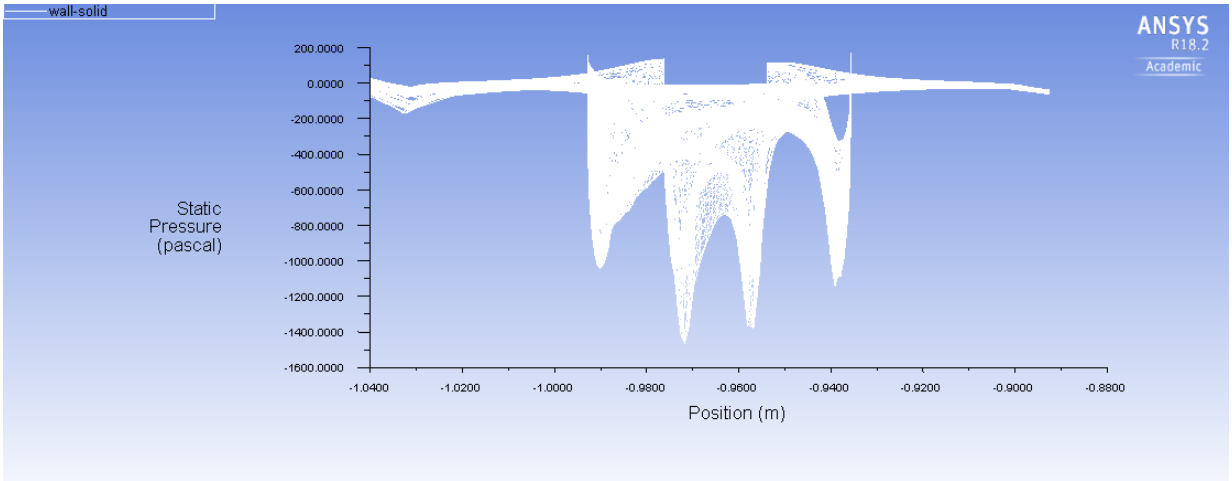

Figure 5.2.6: Model A wall pressure distribution

With the found values for the pressure and the skin friction drag, the drag of the entire camera module was found. In the steps leading up to finding the drag of the camera modules, the drags were found separately to make it easier to find issues in the analysis being followed through for finding the drag. Now, with the found C_d values, and the values of drag found, further discussion can be had on the skin friction and pressure drags of each of the camera modules in the redesign section of this report.

To keep in mind going forward, the frictional drag is important for attached flows where there is no separation. Although this flow is turbulent, it is possible that although there is separation, it may be so little that it can be negligible. This was the case for all three of the side mirrors analysed as the symmetrical geometry of the profiles allowed for the flow to stay relatively attached at the high Reynold's numbers. For this reason, frictional drag played a larger role in the contribution of drag.

On the other hand, pressure drag is important for separated flows and is related to the cross sectional area of the body. All of these shapes had very small cross-sectional areas and therefore also had very small pressure drag values. This can also be seen by the low C_d values found.

5.3 K-Omega Turbulence Model

For the sake of comparison between the two turbulence models, Model A was modelled using the K-omega turbulence model as well as the K-ϵ. As can be logically expected, the two drag values are almost the same. From this, it can be seen that the analysis did not differ much from having chosen one method over the other. The contour for this turbulence model can be seen below in 5.3.1.

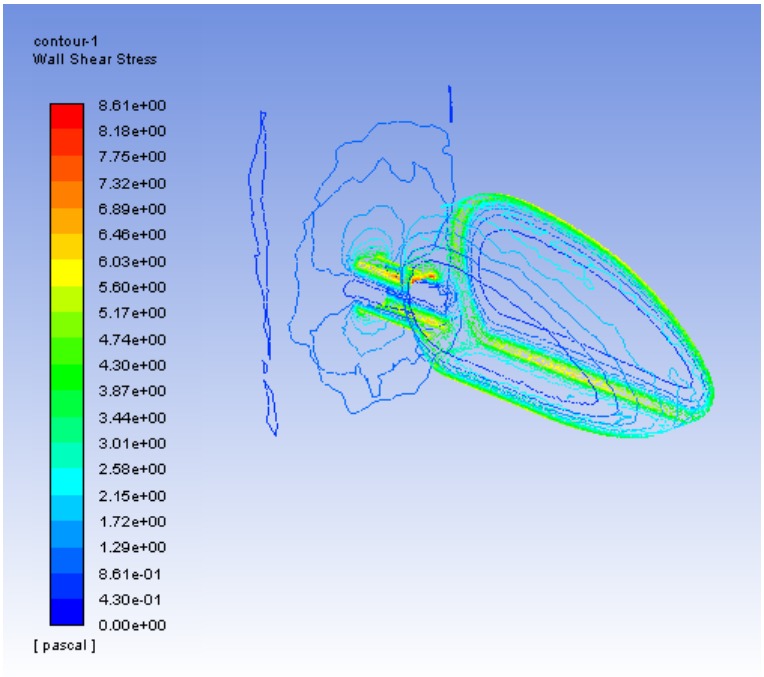

Figure 5.3.1: Contour illustrating the wall shear across surface of mirror, Model A

In table 5.4 is the found drag and drag coefficient values for this turbulence model.

Table 5.4: Drag Values of Model A using K-ϵ and K-ω turbulence models

	K-ϵ	**K-ω**
Drag (N)	3.985	3.751
C_d	0.38	0.3

With the values for the drags found, a discussion can now be had on ways to better the designs of camera side modules for the purposes of drag reduction.

Chapter 6

Re-design

6.1 Aerodynamic Benefits: The Bigger Picture

Looking at the values found so far in this analysis, it is clear that the side camera modules have significant aerodynamic benefits when compared to the traditional solid state side mirror counterparts. It however has not yet been discussed what these drag benefit really mean to a consumer or the manufacturer from an engineering standpoint. Do these benefits warrant for the replacement of traditional side mirrors? Are the benefits enough for them to matter? These are questions which will be answered in this section. First, a look into how the current side mirrors can be redesigned will be had.
Before the redesign process, it is important to know the limit to which the side mirror design can be changed and the benefit it will have on the entire car. Using the Honda Fit for example, the car which Model A Side Mirror is based on, the ideal design benefits can be analysed.

Disclaimer: It also needs to be pointed out that this redesign process is only made possible because of the small space that cameras need to be mounted onto a car. The redesign of a physical solid state side mirror would prove to be much more difficult due to the rules and regulations governing the dimensions that a side mirror is required to be [5]. On the other hand, the camera module can be as small as technologically possible. For this redesign process, there will be no boundary placed and should be noted that the dimensions being tested with may not be feasible to achieve with today's camera technology. However, as camera technology and camera sizing is not a priority in this report, this shall be overlooked.

6.2 Changing the frontal area

Reasoning Changing the frontal area will effectively reduce the pressure drag encountered by the camera module.

Reduction of the frontal/cross sectional area will allow for a decrease in the pressure drag which is experienced by the side mirrors. This is because the lower the cross sectional area, the less likely it will be for the flow to separate (considering all other geometrical parameters to remain the same). For example, in the case of Module C, the cylindrical/rectangular prism shaped module, a reduction in the cross sectional area will see a

reduction in the overall pressure drag which will be experienced by the module. The results from this test are tabulated below in table 6.1.

Table 6.1: Improving upon Model C design

	Initial Design	**Reduced Cross Sectional Area**
Drag (N)	0.857	0.800
C_d	0.365	0.359

The reduction in the cross sectional area of the cylindrical/rectangular part of the side mirror was reduced by approximately 30% while ensuring that the total surface area remained relatively the same. This was done by elongating the shape in the flow direction. Below is a diagram depicting the model in figure 6.2.1. To ensure a reduction in the cross sectional area, the height was simply reduced while increasing the length in the direction of the flow. This effective ensured that while the cross sectional area was being reduced, the surface area of the shape was remaining constant

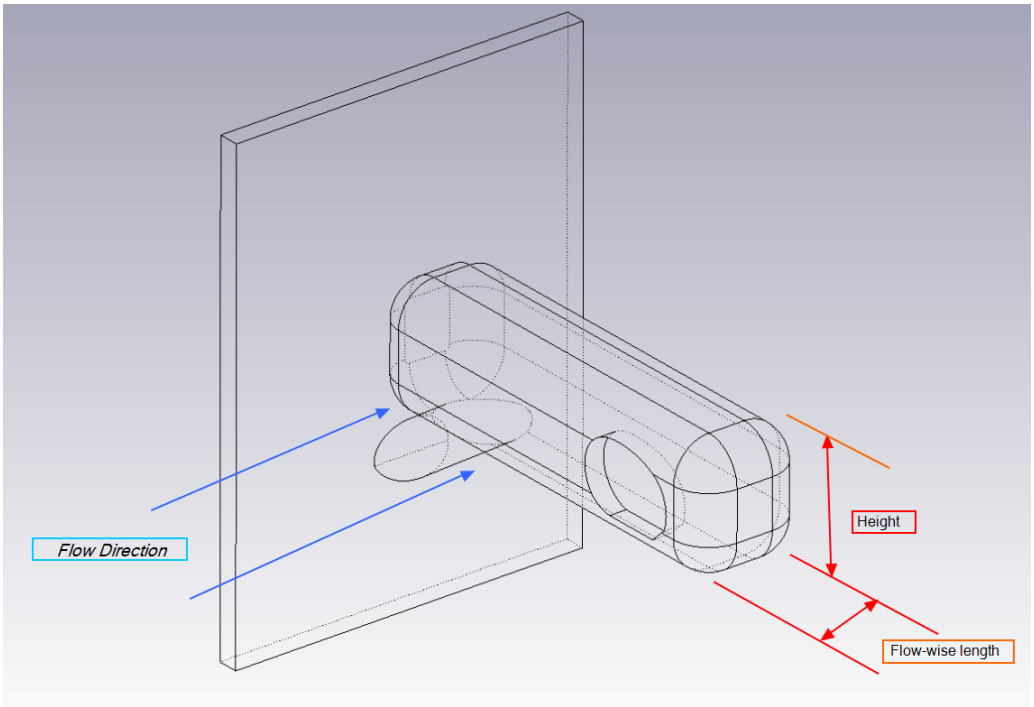

Figure 6.2.1: Model C module used for re-design

It was initially assumed this reduction would see a large decrease in the drag values, however, this was not the case. This is for two main reasons, as listed below.

- The connecting geometry is unchanged
- The model does not experience too much pressure drag.

Firstly, although the geometry for the majority of the camera module was being changed, the camera module's "stem" remains constant. This can be seen illustrated in figure 6.2.1 on the left side of the image connecting the main rectangular shaped body to the plate. This stem may be responsible for a great portion of the drag due to it being a blunt object at an asymmetrical angle in the flow.

The second reason, and the reason more likely, is the fact that this body simply does not experience too great of a pressure drag force. Since this body already has a low C_d value, most of the drag must be coming from skin friction. As observed in the ANSYS simulations, there does not seem to be much separation. This leads to the possibility that rather than a reduction in the pressure drag, a reduction in the skin friction drag for the system will be more effective in reducing the total drag experienced by the camera module.

6.3 Reducing the Surface Area

Reasoning Reducing the overall surface area will reduce the skin friction drag experienced by the camera module. For this analysis, the Honda E, Model B, side mirror module will be analysed. For starters, this is the smallest in surface area of the three side mirrors which were analysed in this report. It is therefore safe to assume that the skin friction of this camera module is the lowest given that the materials for the three camera modules were assumed to be the same. Model B is shown in figure 6.3.1.

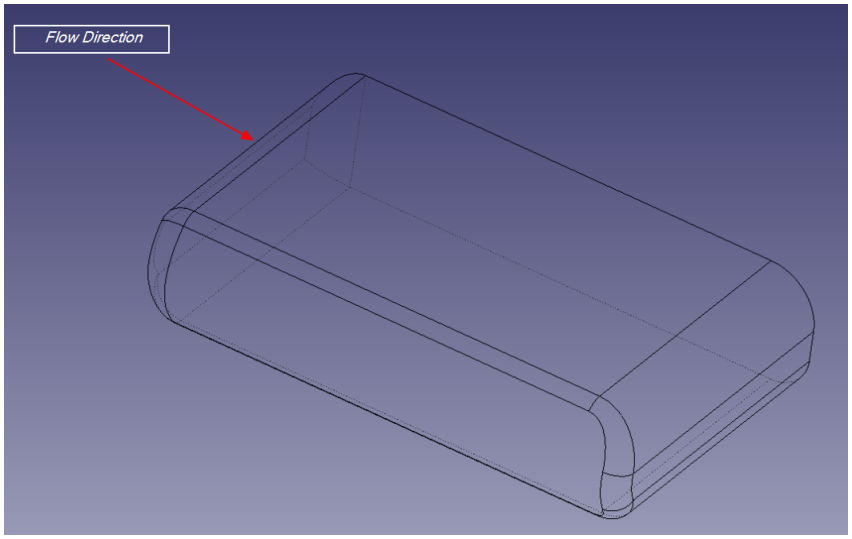

Figure 6.3.1: Model B module used for re-design with the arrow representing the direction of the airflow

For simplicity, Model B was simply reduced by decreasing the overall size with no consideration on the cross sectional area. This should not be an issue as was seen in the previous section where the pressure drag did not play a large enough role for there to be any noticeable change in the overall drag. Therefore, in this case, if there is a large change in the drag, it will be due to skin drag rather than viscous drag.

Table 6.2: Improving upon Model B design

	Initial Design	**Reduced Surface Area**
Drag (N)	0.5260	0.410
C_d	0.312	0.313

For the computation, the overall surface area was reduced by 30%. Due to the proportionality between the surface area and the drag in the calculation of skin friction drag, it can therefore be expected for the total drag to decrease by approximately 30% considering there is very little pressure drag. This was proved to be the case where this reduction in surface area effectively decreased the overall drag of the camera side module by around 21%. This can be seen tabulated above in table 6.2.

As expected, the C_d for the module did not change. This is simply because the drag coefficient is based on the geometry of the object in the flow and not the size. However, as the wetted area/total surface area of the solid is changed, a corresponding decrease in drag can be observed correlating to the decrease in friction. This proves to be a better way of reducing the drag of these peripheral side mirrors.

6.4 Redesign Summary

Tying these points together to the introduction of this chapter, what do these findings mean for the overall vehicle? To answer this question, a similar study can be analysed [16].

In this study, Dr Abdulkareem analysed a Perodua Myvi and its side mirrors with coefficients of drag of 0.354 and 0.175 for the vehicle and the mirrors respectively. This study displayed that the total removal of the mirrors reduces the total vehicle drag coefficient by 4.9%.

This reduction in the total vehicles drag coefficient is very insignificant considering a reduction in the drag coefficient of 0.01% amounts to a increase in the vehicles fuel economy by 0.1 mpg. Even this maximum reduction via removal of the side mirror all together in the drag coefficient simply means that the car will save at most 0.2 gallons per mile.

Therefore, there does not seem to be a greater purpose to the over-engineering of side mirrors for the benefit of drag reduction.

Honda E, with its new side mirror have proudly claimed that their new mirror would reduce the drag compared to conventional mirrors. However, this claim fails to analyse how little a drag reduction of 90% on a small part has on the car as a whole. Therefore, although benefits are in place for the reduction of drag, it is so minuscule that efforts for the re-engineering of other car parts would be more beneficial.

A study done by Ford [17] looked into new technologies being developed by automotive companies for the increase of fuel economy in consumer cars. In this report, Ford outlined parts such as the car rear wing, length of car, vortex generators, car underbelly, bonnet modifications, rear diffuser, and the list goes on. What however is not a priority on their myriad of researched car parts for optimization are side mirrors. This is simply because the drag benefits from the improvement of car side mirrors do not merit millions of dollars being spent on research and development. Instead, this seminar illustrated Ford's interest in the redesign of the vehicle underbelly and front grill as they represent a majority of

the car's drag (30%+ and 14% respectively). Ford also boasts in this report saying that their new technologies implemented to their underbelly and wheel arches can improve the car's fuel economy upwards of 20%.
A brief look through BMW's expenditure on the improvement of fuel economy in their vehicles also show similar findings such where the large portion of their RD goes to the improvement in design of the underbelly and the wheels of the vehicle. Their RD breakdown in fuel economy improvement as of 2010 is as seen tabulated in table 6.3 [17].

Table 6.3: Breakdown of research down by BMW on vehicle drag reduction

System	Percentage of Improvement Opportunities
Upper Body	40
Cooling Drag	10
Under body	20
Tire/wheel/wheel arch	30

With that all being said, it would be recommended that car manufacturers put money into research in other sectors than in the redesign of car side mirrors as the benefits are not as great as Honda makes them seem they are [5].

Pertaining to the matter of the conventional side mirror and the camera modules, the camera modules simply do not offer a great enough drag reduction to warrant companies to make the switch. In addition, there simply is no need to redesign the side mirrors as regulations governing the side the mirror has to be, the angle it must face the driver, the surface area of the mirror and way it is mounted to the car, all limit engineering freedom in increasing the aerodynamics of this part greatly. Parts such as the rims of the car or the underbelly, both parts with which the driver does not directly associate, have freer guidelines and therefore can be engineered with greater leniency. With all this taken into consideration, efforts for fuel reduction in the car should be focused elsewhere.

6.5 Factors not Considered

Although an attempt was made to have a complete analysis into this project, there are several tests and considerations which were not taken into consideration for the purpose of simplicity, a shortage of time, or an educated guess into why such an issue was not of a major concern. Some of these factors which were not considered will now be briefly mentioned. Other factors which have already been discussed in the various sections of the report will not be revisited here.

Modelling at different velocities

For the analysis in this report, the models were all tested at 60 km/h. Since this is the speed that car's drive at in city driving conditions, this was picked as the speed to test the models at. However, a speed of 40 km/h or 100 km/h would be equally as applicable as speeds to have tested at. The lower and higher velocities would have given the chance to observe differences in the pressure drag as the pressure drag tested in the 60 km/h case was very low. For this reason, it would have been interesting to have seen if the amount of separation would drastically increase moving from 60 km/h to 100 km/h. However,

this is slightly unlikely because the flow being observed in all these three models were turbulent and therefore already incorporated mixing. The pressure drag would indeed have been higher at the higher velocity.

The reason as to why this was not done was simply because there was not enough evidence suggesting that a change in velocity would drastically change the outcome of the results. Although the drag would be computed to be higher, it is unlikely that the pressure drag would become larger than the skin friction drag, nor would the drag coefficients vary that drastically. Therefore, to save time on the CFD modelling, the tests were all done at one velocity.

Modelling at different incoming angles of attack

If the angle of attack between the incoming airflow and each side mirror were to be changed, then the values of drag computed would be slightly different. Since the drag calculated is parallel to the direction of the flow, having an angle to which the air is flowing over the mirror modules would mean that the drag being calculated would only be a portion of the total drag.

Although this would reduce the drag, the drag component in the direction of the flow would still most likely be almost the same as the magnitude of the flow itself. This is because in the modelling of the car, it is unlikely that the incoming airflow would be drastically inclined simply because cars drive parallel to the road and the air flows parallel to that. In in-climate conditions or when driving uphill for example, there may be cases where the drag is drastically changed on the side mirrors momentarily, but, for the most part, the air flows over the side mirror parallel to the car's body's orientation.

Using manufacturer designed CAD models

The CAD models used in this design were based off estimations. Meaning, none of these models were provided for the conduction of this thesis paper. For this reason, there is room for error in the modelling of each part, and therefore the analysis as a whole. The main reason for this is because manufacturers do not make accurate CAD files available to the public as that would leak secrets to competitors.

However, this did not prove to be an issue the values found for each of the three camera modules agreed with engineering literature and can therefore be said to have been accurate representations of the physical models used by the automobile manufacturers. Coincidentally, there may have also been cases where slight defects in the way that the author modelled the part in one section balanced out an oversimplified portion of the design on another section, resulting in a drag coefficient and drag values which agree with those found in literature. Nonetheless, as the real CAD models were not available, an effort was made to replicate them as accurately as possible.

Costs associated with side mirror camera modules

This thesis looks at the pros and contras of camera modules and a conventional side mirror but it did not look into the price differences between the two modules. It can be assumed

that the conventional side mirror will be cheaper to install, cheaper to maintain, and cheaper to replace than one which has a built in camera. For example, the replacement of a conventional side mirror can be done independently with screws and a screwdriver and a purchase of the required part off an online store. A camera module however, would most likely require the assistance of a trained professional costing more money, and requiring more time out of the consumer.

Although cost is a very important consideration, the reason it was not delved into detail into is because cost fluctuates greatly overtime. As the side mirror camera modules are a new technology, it is likely that the price to maintain and buy such equipment are expensive. But given a handful of years, these parts will be plentiful and may even overrule the conventional side mirrors currently on the market. Therefore, even though the price may rule against the camera modules today, in a few years, the balance may be shifted. In addition, if the conclusion to this thesis was that there is a reason to switch to the camera modules rather than the conventional side mirrors, a trade study would have to be done comparing the pros and cons of having made this replacement. However, this thesis did not take such a route.

6.6 Conclusion

This thesis was written with the purpose of reducing drag on an automobile by the optimization or replacement of traditional side mirrors. For this study, CFD modelling on three parts were done: a traditional side mirror, and two existing camera modules to replace the conventional part. Seeing as the manufacturers of these technologies proudly present their new creation at autoshows and car events, it was expected in this thesis that these new camera modules would have aerodynamic improvements which far exceed their predecessors. This was not this case.

Through analysis, the results suggest that regardless of the detail in the redesign process, the benefits from having a new camera module to replace the conventional side mirror are very small. The benefits are so minuscule in fact, that even the removal of side mirrors all together have proven to have only an improvement of approximately 0.2 mpg. Therefore, although benefits in the camera module include increased safety due to better viewing angles, they simply do not add enough aerodynamic benefits for them to replace traditional solid state side mirrors. In addition, there simply is no need to redesign the side mirrors as regulations governing the side the mirror has to be, the angle it must face the driver, the surface area of the mirror and way it is mounted to the car, all limit engineering freedom in increasing the aerodynamics of this part greatly.

Moving forward, it can be concluded that car manufacturers should invest their money elsewhere in search of ways to increase the car's fuel economy rather than in the redesign of car side mirrors.

Bibliography

[1] ANSYS. Modelling turbulence. https://www.afs.enea.it/fluent/Public/Fluent-Doc/PDF/chp10.pdf, 2013.

[2] Sighard .F Hoerner. *Fluid-Dynamic Drag*. 1965.

[3] Mohammad Ali Quamrul Islam S.M Rakibul Hassan, Toukir Islam. Numerical study on aerodynamic drag reduction of racing cars. https://reader.elsevier.com/reader/sd/pii/, 2014.

[4] James Fossdyke. Honda e to get side camera mirror system as standard. https://www.motor1.com/news/351805/honda-e-side-cameras-standard/, 2019.

[5] Sean Szymkowski. Nhtsa wants your input on camera-based side mirror technology. https://www.cnet.com/roadshow/news/nhtsa-side-mirror-camera-technology/, 2019.

[6] Efstathios E. Michaelides Sabine Tran-Cong, Michael Gay. Drag coefficients of irregularly shaped particles. *Powder Technology*, 139:21–32, 2003.

[7] Wikipedia. Skin friction drag. https://en.wikipedia.org/wiki/Drag_equation, 2019.

[8] Snorri Gudmundsson. Skin friction coefficient. https://www.sciencedirect.com/topics/engineering/friction-drag-coefficient, 2008.

[9] Ansys. Turbulence modeling for cfd simulation. https://www.ansys.com/products/fluids/turbulence-modeling, 2020.

[10] Shawn Wasserman. Choosing the right turbulence model for your cfd simulation. https://www.engineering.com/DesignSoftware/DesignSoftwareArticles/ArticleID/13743/Choosing-the-Right-Turbulence-Model-for-Your-CFD-Simulation.aspx, 2016.

[11] OpenFoam. Realizable k-epsilon. https://www.openfoam.com/documentation/guides/latest/doc/guide-turbulence-ras-realizable-k-epsilon.html, 2016.

[12] Tomer Avraham. Know thy mesh-mesh quality. https://allaboutcfd-tomersblog.com/2019/02/01/know-thy-mesh-mesh-quality-part-i/, 2019.

[13] ANSYS. Monitoring residuals. https://www.afs.enea.it/project/neptunius/docs/fluent/html/ug/node812.html, 2009.

[14] S.P. Sukhatme. *A textbook on Heat Transfer*, volume 4. 2005.

[15] Eco Modder. Vehicle coefficient drag list. https://ecomodder.com/vehicle_coeff, 2018.

[16] Abdulkareem Sh. Mahdi Al-Obaidi. Effect of size and shape of side mirrors on the drag of a personal vehicle. *International Engineering Research Conference*, 7, 2016.

[17] Neil Lewington. Aerodynamics fundamentals for automotive. *SAE-Australasia*, 2005.

Chapter 7

Appendix

7.1 Drawings

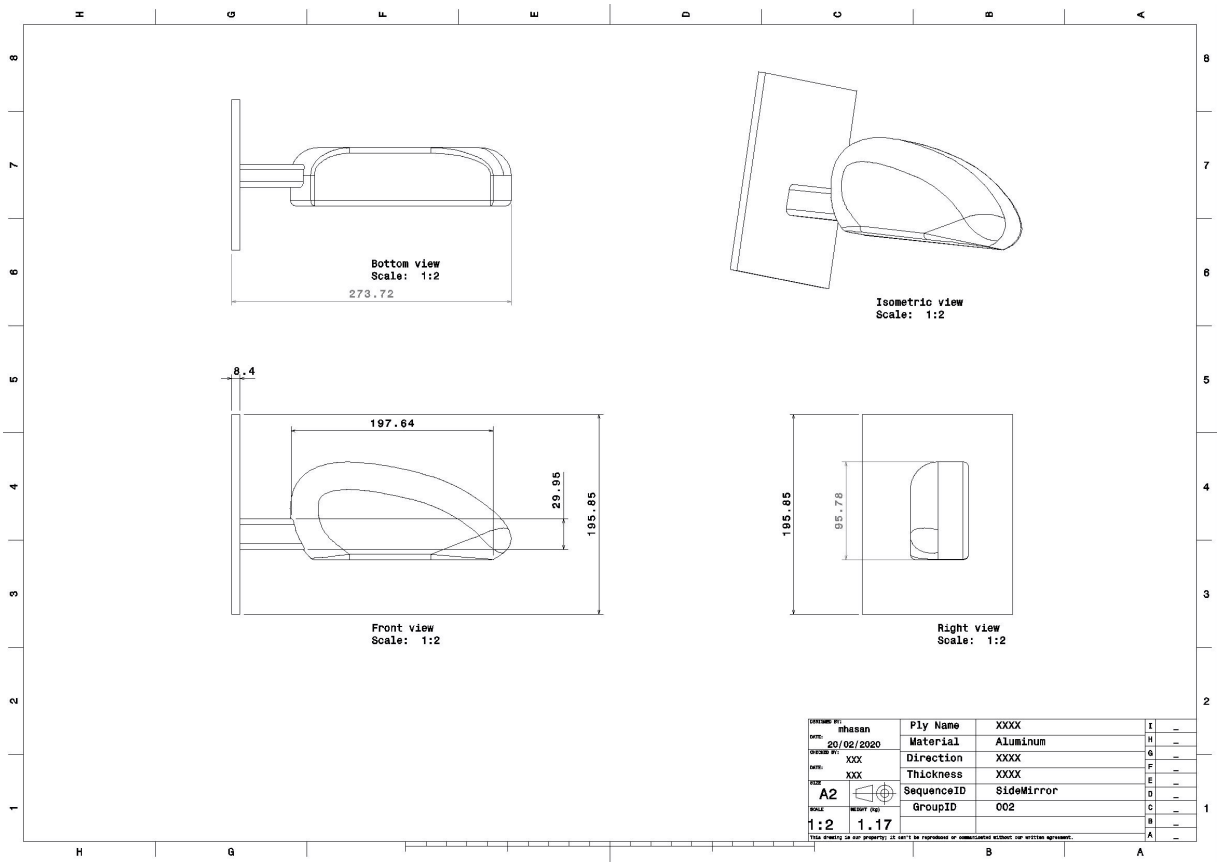

Figure 7.1.1: Generic Automobile Car Side Mirror

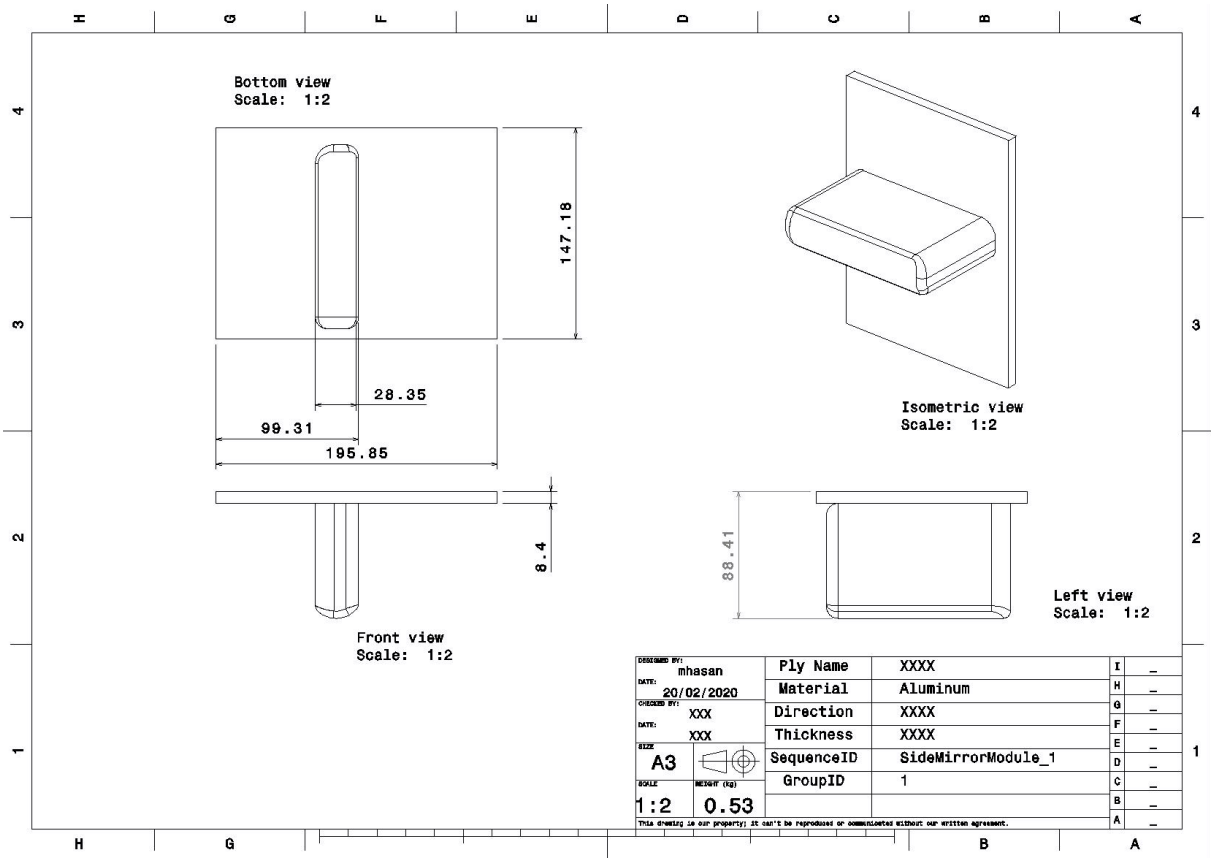

Figure 7.1.2: Honda E Side Mirror Drawing, Model B

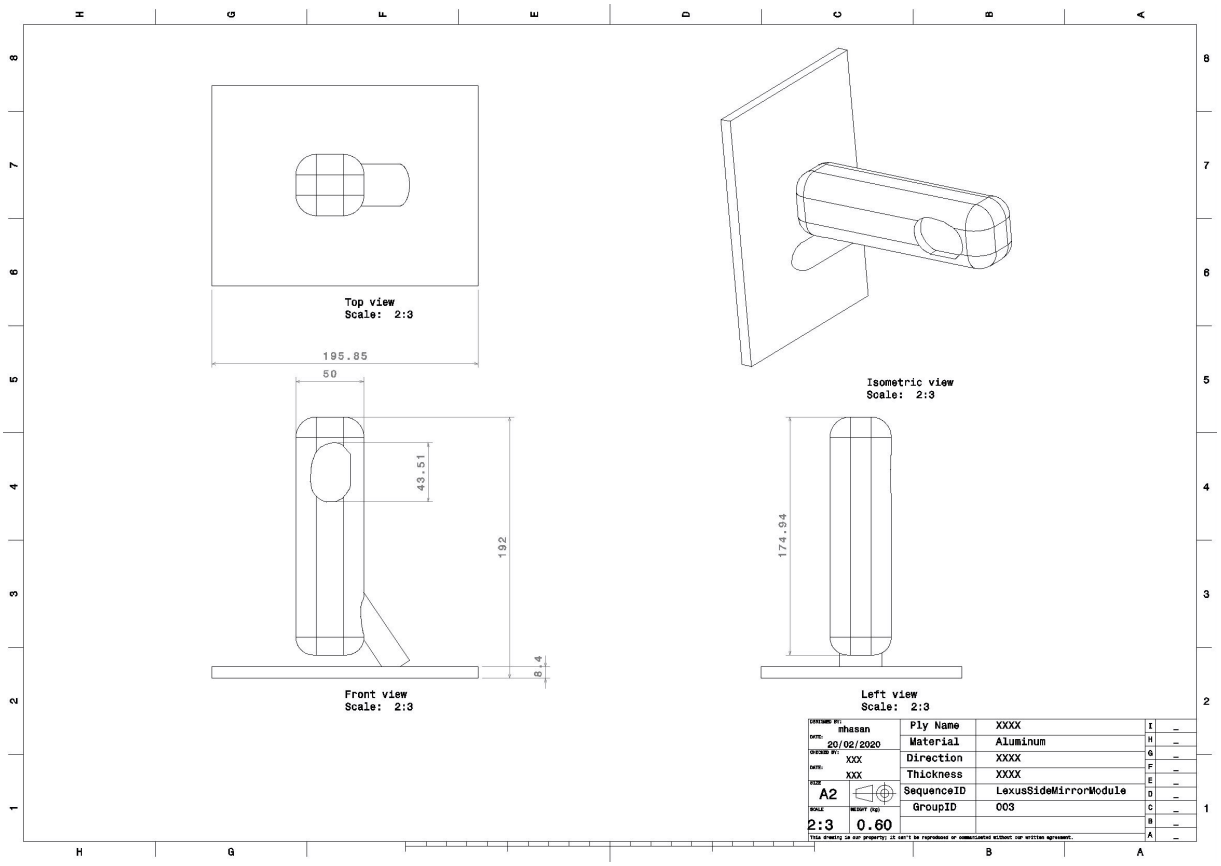

Figure 7.1.3: Lexus Side Mirror Drawing, Model C